Comparison of local electrochemical impedance measurements derived from bi-electrode and microcapillary techniques

Jean-Baptiste Jorcin[a], Halina Krawiec[b,*], Nadine Pébère[a], Vincent Vignal[c]

[a] Université de Toulouse, CIRIMAT, UPS/INPT/CNRS, ENSIACET – 118 route de Narbonne, 31077 Toulouse Cedex 04, France
[b] AGH, University of Science and Technology, Reymonta 23 Street, 30-059 Krakow, Poland
[c] ICB, UMR 5209 CNRS - Université de Bourgogne, BP 47870, 21078 Dijon Cedex, France

ABSTRACT

In the present paper, local electrochemical impedance spectra were obtained on a 316L stainless steel from two configurations: a dual microelectrode (bi-electrode) and microcapillaries. With the bi-electrode, the local impedance measurements were made from the ratio of the applied voltage to the local current density calculated from the application of the ohm's law. With the use of microelectrochemical cells, the specimen surface area in contact with the electrolyte is limited by the use of glass microcapillaries and the local impedance was defined from the ratio of the local potential to the local current restricted to the analysed surface area. Differences and similarities observed in local impedance spectra obtained with the two configurations were described.

1. Introduction

Conventional electrochemical impedance spectroscopy is used since more than 40 years for studying electrochemical mechanisms occurring at the electrode/electrolyte interface. However, this technique is limited to surface-averaged measurements which account for the behaviour of the whole electrode surface. In corrosion problems, such as in localized corrosion, the response associated with local phenomena (pitting, crevice corrosion, breakdown of the passive film, etc.) cannot be extracted from the global impedance diagrams. To overcome these difficulties, several scanning techniques using microelectrodes have been developed. Among them, the local electrochemical impedance spectroscopy performed on restricted active areas was pioneered by Isaacs et al. [1–3]. The local impedance was obtained with the use of a dual microelectrode which measured the local ac-potential, the local current being calculated from the application of the Ohm's law [2–4]. With bi-electrodes, Annergren et al. [5] have obtained local impedance diagrams over an active pit and the results were compared with the global impedance. Using larger probes, Philippe et al. [6] investigated polymer-coated galvanized steel whereas Baril et al. [7] studied the electrochemical behaviour of an AZ91 magnesium alloy. More recently, the same experimental set-up was used to investigate the initiation and propagation of delamination at the steel/organic coating interface [8] and also to determine the extension of sensitized zones in welded AISI304 stainless steel [9]. Moreover, in a recent series of papers, Huang et al. [10–12] have undertaken an analysis of the LEIS technique when it is applied to a disk electrode. The major conclusion is that the calculated and experimentally observed frequency dispersion and imaginary contributions to Ohmic impedance were attributed to the current and potential distributions associated with the typical geometry of the disk electrode.

Since the mid-1990, another local approach was proposed which consisted in using microcapillaries as electrochemical cells and thus in another way to decrease the analysed surface areas [13]. The electrochemical microcell technique allows the selection and interrogation of single metallurgical sites and is therefore becoming increasingly popular to investigate the electrochemical behaviour of metallic phases and non-metallic heterogeneities in alloys. It has been shown that there is a good correlation between the pitting resistance equivalent number (PREN) and the pitting susceptibility of metallic phases in duplex stainless steels [14,15]. The basic parameters describing both pitting corrosion mechanisms in aluminium alloys [16,17] and the electrochemical dissolution of MnS inclusions [18–24] and CrN [25] (formed at temperatures between 700 °C and 900 °C) in stainless steels have also been evaluated in various electrolytes. In addition, the influence on the electrochemical behaviour of materials of strain gradients induced by surface preparation [26] and wearing [27] have been quantified at the microscale. Recently, the local polarisation curves obtained from

Corresponding author. Tel.: +48 12 6172763; fax: +48 12 6336348.
E-mail address: krawiec@agh.edu.pl (H. Krawiec).

microcapillary cells have been compared with numerical calculations derived from a model using a finite element approach [28]. It has been shown that some parameters, such as the microcell crevice geometry and the specimen surface–capillary gap distance, lead to significant modifications of the curves. In contrast, only a few papers have reported the use of the electrochemical microcell technique to perform impedance measurements in the micrometer scale range. Some special strategies and examples of this micro-impedance spectroscopy have been presented and discussed in Refs. [29–31].

In the present paper, the local electrochemical impedance diagrams obtained from both bi-electrode and microcapillaries are compared. The aim is to emphasize the sensitivity and the limits of the two configurations. Experiments were performed on a stainless steel (316L type). The material was chosen because it is a monophasic material without any inclusion. The electrochemical parameters were obtained from a fitting procedure of the local impedance diagrams and were compared with those obtained from global (conventional) electrochemical impedance diagrams used as reference. The electrolyte concentrations were chosen in order to easily compare the local impedance results.

2. Experimental

2.1. Electrochemical measurements

2.1.1. Global electrochemical impedance measurements
Global electrochemical measurements were carried out using a classical three-electrode cell: the working disk electrode (2.5 cm in diameter) insulated by coating with a cataphoretic paint and embedded in an epoxy resin, a saturated calomel reference electrode (SCE) and a platinum auxiliary electrode. An AutoLab PGZ32 electrochemical interface/frequency response analyser was used in these experiments. Diagrams were plotted in a frequency range of 65 kHz to a few mHz with four points per decade using 10 mV peak-to-peak sinusoidal voltage.

2.1.2. Local electrochemical impedance measurements with the bi-electrode technique
With the bi-electrode technique, local impedance measurements were carried out on a 0.9 cm diameter disk with a Solartron 1275. This method uses a five-electrode configuration and details can be found in Ref. [8]. The principle of the technique is recalled briefly: LEIS measurements are made from the ratio of the applied AC voltage to the local AC current density. The applied voltage ($\Delta V_{applied}$) is the potential difference between the working electrode and the reference electrode. The local AC current density (i_{local}) is calculated using the Ohm's law:

$$i_{local} = \frac{\Delta V_{local}}{d} \kappa \tag{1}$$

where κ is the conductivity of the electrolyte and d is the distance between the two probes. The local impedance Z_{local} is calculated by the relationship:

$$Z_{local} = \frac{\Delta V_{applied}}{i_{local}} \tag{2}$$

The local impedance diagrams were recorded over a frequency range of 10 kHz to around 100 mHz with six points per decade. The diagrams were obtained at three positions along the electrode radius: at the centre ($r/r_0 = 0$), at $r/r_0 = 0.4$ and at $r/r_0 = 0.8$. With the used experimental set-up (probe geometry), only the normal component of the current was measured and the spatial resolution was roughly estimated to be about 1 mm^2 for each measurement [32].

2.1.3. Local electrochemical impedance measurements with the use of microcapillaries
The size of the microcapillaries was chosen to have comparable surface areas as that analysed by the bi-electrode technique and, thus, experiments were carried out with 250 μm and 480 μm microcapillaries. The microcapillary tip was sealed to the specimen surface with a layer of silicon rubber (in order to avoid leakage and crevices). In addition, a high resolution and low noise potentiostat/frequency response analyser was used to detect currents in the limit of 30 pA (AutoLab PGZ32). The diagrams were obtained over a large frequency range (100 kHz to 10 mHz), with five points per decade.

2.2. Specimens and surface preparation

Measurements were performed on a 316L stainless steel (chemical composition (wt.%): Ni: 11.04, Cr: 16.67, Mn: 1.53, S: 0.025, Si: 0.42, Mo: 2.26, P: 0.025, C: 0.018 and N: 0.07). Specimens were mechanically grounded with silicon carbide (SiC) emery papers down to 4000 grit, polished with diamond pastes down to 1 μm, washed by water and then ultrasonically rinsed in ethanol.

Both global and local electrochemical impedance measurements were performed on the stainless steel sample in 0.1 M, 0.01 M and 0.001 M NaCl solutions, after 90 min of immersion at the open circuit potential (OCP). This immersion time allowed the corrosion potential to be stable and thus to avoid dispersion of the low frequency points.
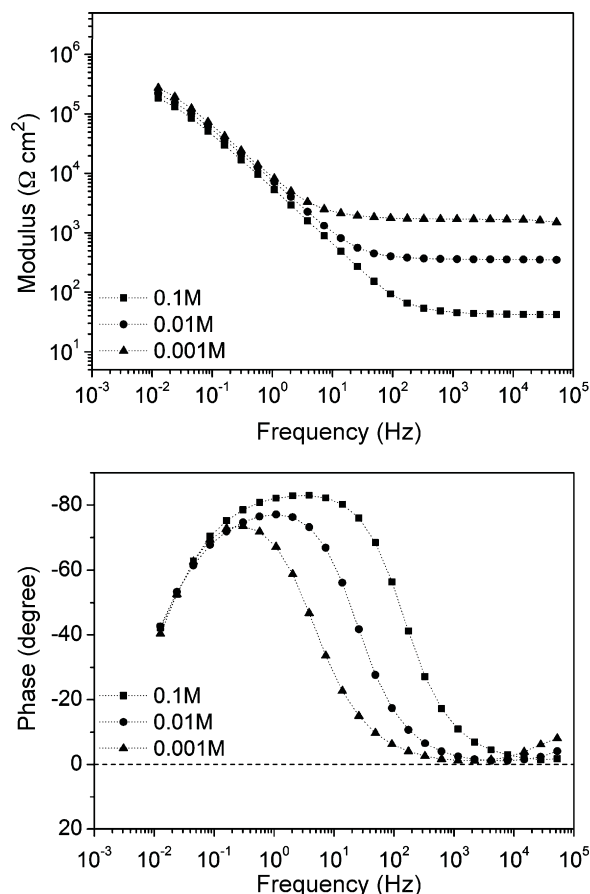

Fig. 1. Electrochemical impedance diagrams (Bode representation) obtained for the stainless steel disk in electrolytes containing sodium chloride at different concentrations: (■) 0.1 M, (●) 0.01 M and (▲) 0.001 M.

2.3. Impedance data analysis

Impedance data were analysed using the Z-plot/Z-view software package and fitted to the appropriate equivalent circuit.

3. Results and discussion

Global and local impedance results are presented here for the stainless steel in different NaCl concentrations. Different NaCl concentrations were chosen because usually LEIS measurements with the bi-electrode are performed in a low conductivity medium (0.001 M) to improve the resolution of the method (the measured local current depends on the conductivity of the electrolyte). Conversely, LEIS measurements with microcapillaries need high conductivity media (0.1 M or higher) due to the very low measured current (small analysed surface area). Thus, the three chosen con-

centrations allow the whole domain of electrolyte concentrations currently used for both configurations to be covered and as a consequence to evaluate the sensitivity and the limits of each local technique (when the concentration is increased (bi-electrode) or is decreased (microcapillaries)). The local diagrams obtained by the two configurations will be analysed and compared with the global impedance diagrams which constitute the reference.

3.1. Global impedance

Fig. 1 shows the Bode representation of the global impedance responses for the stainless steel in the different NaCl solutions. The impedance response of the sample is that of an electrode coated by a passive oxide film. For the three concentrations, the low frequency (LF) part of the diagrams (frequencies below 1 Hz) is superimposed whereas the high frequency part differs accord-
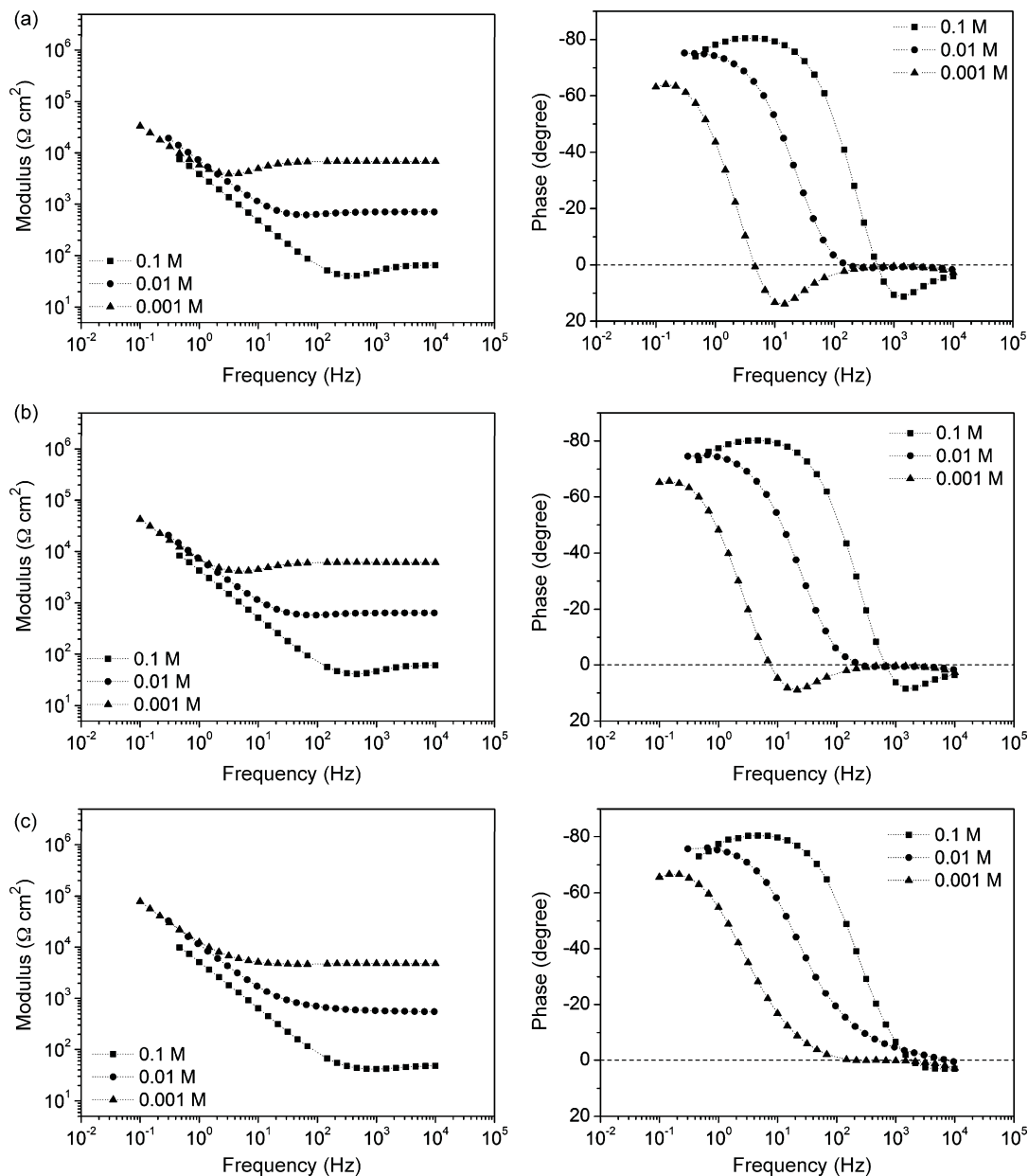

Fig. 2. Local electrochemical impedance diagrams obtained with the bi-electrode (Bode representation) for different positions of the probe along the stainless steel electrode radius (a) at the centre ($r/r_0 = 0$), (b) at $r/r_0 = 0.4$ and (c) at $r/r_0 = 0.8$, in electrolytes containing sodium chloride at different concentrations: (■) 0.1 M, (●) 0.01 M and (▲) 0.001 M.

Table 1
Comparison of the parameters associated with the properties of the oxide film obtained from electrical equivalent circuit to analyze the classical and the two types of local electrochemical impedance diagrams (bi-electrode and microcapillaries).

[NaCl]	Set-up	R_{ox} (kΩ cm^2)	Q_{ox} (MΩ^{-1} cm^{-2} s$^\alpha$)	α_{ox}
0.1 M	Conventional impedance	276	33	0.93
	Bi-electrode, $r/r_0 = 0$	455	45	0.93
	Bi-electrode, $r/r_0 = 0.4$	446	41	0.93
	Bi-electrode, $r/r_0 = 0.8$	519	34	0.93
	Capillary, $d = 450\,\mu$m	694	18	0.92
	Capillary, $d = 280\,\mu$m	434	33	0.89
0.01 M	Conventional impedance	360	27	0.90
	Bi-electrode, $r/r_0 = 0$	212	27	0.89
	Bi-electrode, $r/r_0 = 0.4$	220	27	0.89
	Bi-electrode, $r/r_0 = 0.8$	1063	18	0.88
	Capillary, $d = 480\,\mu$m	768	18	0.84
	Capillary, $d = 280\,\mu$m	442	41	0.78
0.001 M	Conventional impedance	308	35	0.91
	Bi-electrode, $r/r_0 = 0$	158	44	0.89
	Bi-electrode, $r/r_0 = 0.4$	217	35	0.89
	Bi-electrode, $r/r_0 = 0.8$	519	19	0.86
	Capillary, $d = 480\,\mu$m	2407	9	0.77
	Capillary, $d = 260\,\mu$m	1397	41	0.79

ing to the electrolyte concentration. The diagrams exhibit a single time constant with high impedance values. The impedance reveals constant phase element (CPE) behaviour. The CPE exponent (α) was determined by plotting the imaginary part of the impedance as a function of frequency in logarithmic scale [33]. A slope of -0.92 ± 0.01 was obtained, which means that the exponent was 0.92 ± 0.01. The value of α was obtained directly without regression of equivalent circuit. The observed time constant is attributed to the oxide film resistance and the CPE coefficient (Q) to the oxide film.

3.2. Local electrochemical impedance (bi-electrode)

Fig. 2 shows the Bode representation of the local impedance diagrams obtained for three positions on the electrode surface: at the centre $r/r_0 = 0$ (Fig. 2(a)), at $r/r_0 = 0.4$ (Fig. 2(b)) and at $r/r_0 = 0.8$ (Fig. 2(c)) and for the three NaCl contents. In the high frequency domain, inductive parts are observed. Such behaviour has been recently explained by calculating the influence of geometry-induced current and potential distributions on the impedance response of a blocking disk electrode [10,11]. The calculated local impedance shows inductive features at high frequency which are caused by the influence of the local ohmic impedance. Thus, the inductive loops are not related to the electrochemical behaviour of the stainless steel surface. Moreover, the influence of the ohmic drop on the local impedances is dependent on the probe position [10–12]. This is better visualised in Nyquist coordinates. As an example, Fig. 3 reports the diagrams for the three probe positions for 0.001 M NaCl. When the bi-electrode was moved from the centre to the edge of the stainless steel disk, the size of the inductive loop first decreased and disappeared on the edge of the disk. In addition, the electrochemical response (low frequency part of the impedance diagram) was dependent on the probe position. The impedance is lowest at the centre of the disk and larger at the periphery. This result can be explained by the fact that only the normal component of the local current was measured [32]. This is better visualised in Fig. 2 and will appear in Table 1 presented later. The obtained results were in good agreement with previous results [11,32]. It can be seen that for the lowest NaCl concentration more points can be obtained in the low-frequency range (until 0.1 Hz for 0.001 M NaCl instead of 0.4 Hz for 0.1 M NaCl) due to the local current which is higher in a low conductive medium.
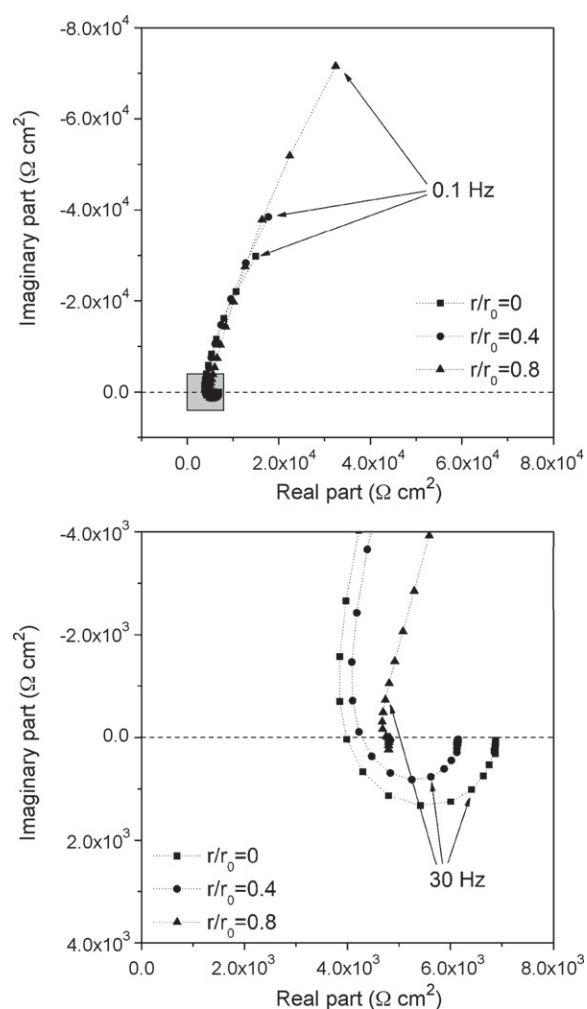

Fig. 3. Local electrochemical impedance diagrams obtained with the bi-electrode (Nyquist representation) for three different positions of the probe along the stainless steel electrode radius (■) at the centre ($r/r_0 = 0$), (●) at $r/r_0 = 0.4$ and (▲) at $r/r_0 = 0.8$, in 0.001 M NaCl.

3.3. Local electrochemical impedance (microcapillaries)

Fig. 4(a) and (b) shows local electrochemical impedance diagrams obtained using the electrochemical microcell technique with $250\,\mu$m and $480\,\mu$m microcapillaries, respectively. The impedance data were corrected by the analysed surface area (in Ω cm^2). For both sets of microcapillaries, a first time constant is visible at high frequencies. The value of the impedance modulus on the plateau decreases as the NaCl concentration increases (roughly $10^4\,\Omega$ cm^2 in 0.001 M NaCl down to $10^1\,\Omega$ cm^2 in 0.1 M NaCl). The first time constant is related to the potential distribution in the microcapillary which depends on the charge distribution. It has been shown [28] that the diffusive flux of species in the microcapillary, and therefore the charge distribution, is not uniform and depends on its geometry (especially at the microcapillary tip which has a conic shape). This effect is exacerbated by the low conductivity of the electrolyte. To avoid this phenomenon, the reference and counter electrodes should be placed as close as possible from the electrode surface. Obviously, from a technical point of view, the microcapillary diameter should be larger to contain the electrodes. In the low-frequency range, a capacitive behaviour was observed. For 0.01 M and 0.1 M NaCl, the impedance diagrams are constituted by two time constants which are poorly separated (better visualised on the phase angle plots).
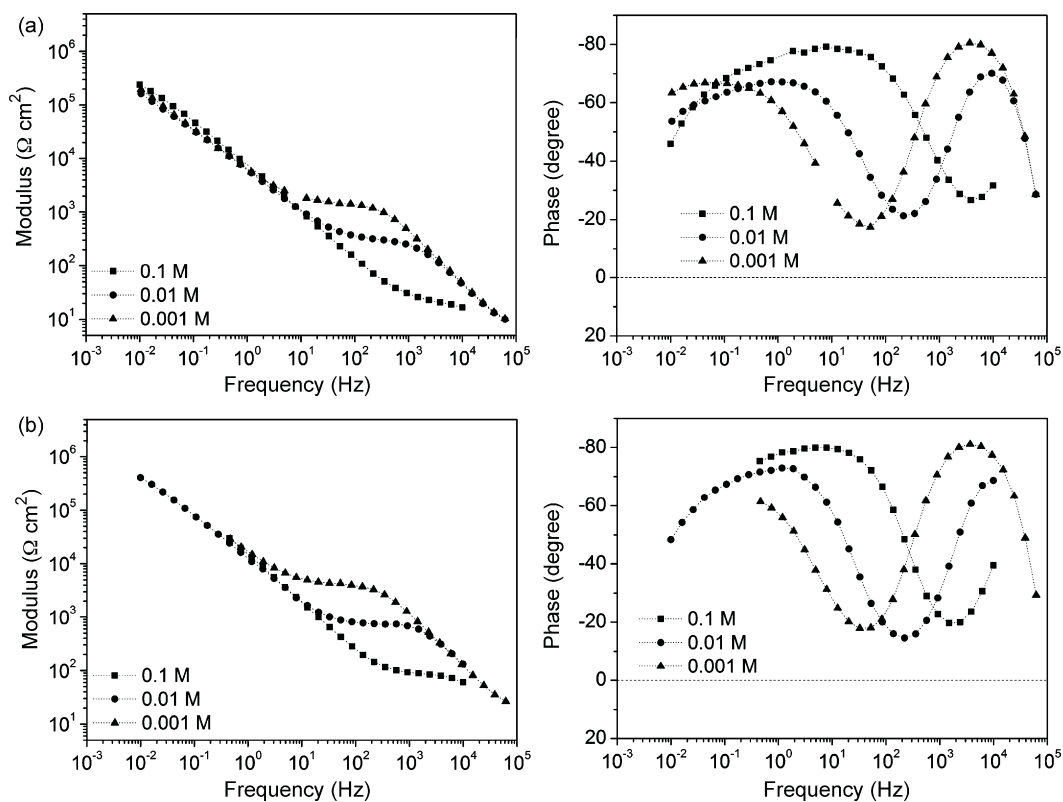
Fig. 4. Local electrochemical impedance diagrams obtained with two capillaries (Bode representation): (a) 250 μm and (b) 480 μm in electrolytes containing sodium chloride at different concentrations: (■) 0.1 M, (●) 0.01 M and (▲) 0.001 M.
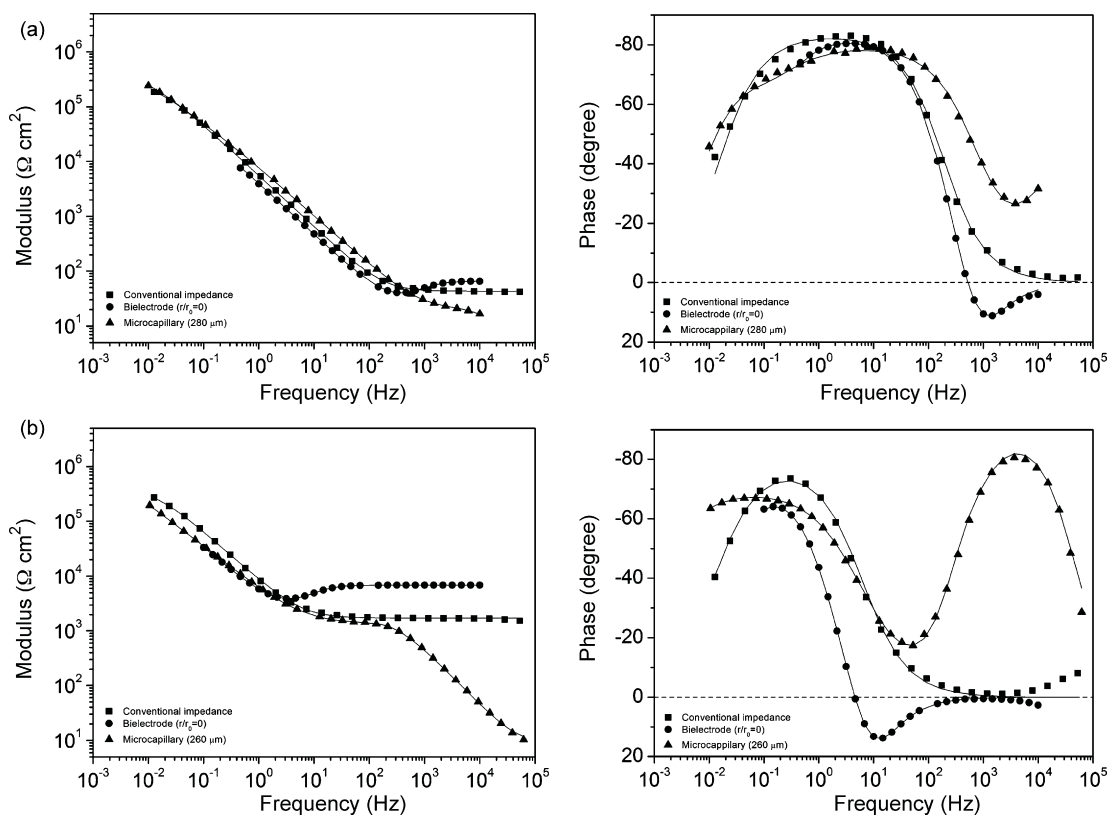

Fig. 5. Comparison of the global impedance diagram and the two types of local electrochemical impedance diagrams obtained with the bi-electrode and the microcapillaries (Bode representation) (a) in 0.1 M NaCl and (b) in 0.001 M NaCl. Continuous lines represent the model data corresponding to the equivalent circuit in Fig. 6.
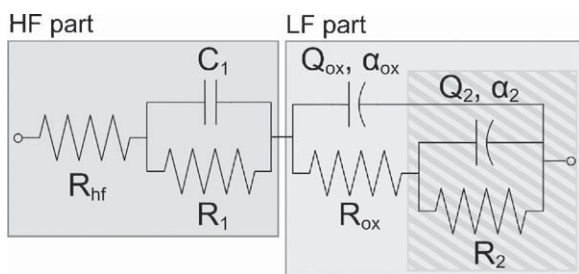
Fig. 6. Electrical equivalent circuit used to analyze both the global and the two types of local electrochemical impedance diagrams obtained with the bi-electrode and the microcapillaries. R_{hf}, high frequency limit of the impedance diagram. C_1 and R_1, parameters associated with the HF time constant observed with the microcapillaries. R_{ox}, resistance associated with the oxide film. Q_{ox} and α_{ox}, parameters associated with the properties of the oxide film. R_2, Q_2 and α_2, parameters which account for the presence of a new time constant in the low-frequency range.

3.4. Comparison of the impedance results obtained from the two configurations

To compare the different results, the diagrams obtained from conventional impedance, bi-electrode and microcapillary (280 μm) are reported in Fig. 5(a) for 0.1 M NaCl and on Fig. 5(b) for 0.001 M NaCl. For 0.1 M NaCl, the major difference between the diagrams appears in the high frequency range (from 10 kHz to 100 Hz). Whereas, in the low frequency domain (below 100 Hz), the diagrams are quite comparable. However, as previously mentioned for the microcapillary, two time constants are visible on the phase angle. For 0.001 M NaCl, the differences are more significant. In the high frequency range (from 8 kHz to 5 Hz) the diagrams are strongly dependent on the technique used. The frequency domain where the diagrams are superimposed becomes very narrow.

A description of the impedance diagrams can be obtained by using an equivalent circuit, presented in Fig. 6. The circuit is divided in two blocks. The first one is associated with the high frequency part of the diagram and the second one to the low frequency part. Only resistances and capacitances (or CPE) were used. R_{hf} corresponds to the high frequency limit of the impedance diagrams. R_1 and C_1 are representative, either of the inductive part (bi-electrode), or of the first time constant in the high frequency range (microcapillary). As previously mentioned, the high frequency part of the diagrams does not bring any information on the electrochemical behaviour of the interface. Experimental conditions (microcapillary size and electrolyte concentration) strongly affect this part of the diagrams. As it can be seen in Fig. 5, when the NaCl concentration increases, the capacitive loop (microcapillary) and the inductive one (bi-electrode) tend to disappear. R_2 (resistance associated with the time constant in the LF range), Q_2 (CPE coefficient) and α_2 (CPE exponent) are added in the equivalent circuit to take into account the presence of the two time constants observed with the microcapillaries: the first one characterized the oxide film and the second one could be linked to the microcapillary configuration (silicon rubber, for example). The experimental diagrams were fitted by the equivalent circuit given in Fig. 6. In Fig. 5, the dotted lines show the fitting results. It can be seen that the model results were quite similar to the experimental data.

R_{ox} (resistance), Q_{ox} (CPE coefficient) and α_{ox} (CPE exponent) are the characteristic oxide film parameters thus compared. The values of R_{ox}, Q_{ox} and α_{ox} obtained from the fitting of the impedance diagrams (Fig. 5) are reported in Table 1. With the conventional impedance, the value of R_{ox} ($\sim$300 kΩ cm^2), Q_{ox} (35 MΩ^{-1} cm^{-2} s$^{\alpha}$) and α_{ox} (0.93) are in agreement with values measured on oxide films [11]. With the bi-electrode technique, R_{ox} is of the same order of magnitude than that obtained with the conventional impedance. However, as previously mentioned, R_{ox} increases from the cen-

tre to the edge of the electrode (Q_{ox} decreases), due to potential distributions. This effect is more marked when the electrolyte concentration decreased. We can mention that the α_{ox} parameter is, independently of the probe position, equal to 0.93 for the 0.1 M NaCl solution and to 0.89 for the 0.001 M NaCl solution. The fact that α_{ox} is lower than 1 (Q is not a real capacitance) account for a 3D distribution in the oxide film [34]. For an oxide layer, the distribution in the direction normal to the electrode surface can be due to varying oxide composition [35]. With the microcapillary and for 0.1 M NaCl concentration, the values of R_{ox}, Q_{ox} and α_{ox} are in good agreement with the values obtained from the other measurements. For 0.001 M NaCl, the R_{ox} values are higher than those obtained with the conventional impedance and bi-electrodes. These results outline that low conductive media are not suitable for microcapillary measurements.

4. Conclusion

Impedance spectra were obtained on a stainless steel disk in sodium chloride media both at the macroscale using the conventional method and at the microscale using bi-electrode and microcapillary techniques. It was shown that the low frequency part of the impedance diagrams obtained with the microcapillaries probably includes the properties of both the oxide film and the microcapillary. This point would need complementary investigations. It was also verified that microcapillaries cannot be used in low conductive media (strong ohmic drop effects). In contrast, microcapillaries appear as the most appropriate technique to do local measurements in highly conductive media in which the frequency domain investigated with the bi-electrode technique is decreased.

Bi-electrodes and microcapillaries can be combined in most of the electrolytes used for corrosion studies (concentration in the range of 0.1–1 M NaCl). Bi-electrodes can be used to perform high resolution mapping of large surface areas defined by a heterogeneous microstructure (assemblies, welded zones, coatings with defects, etc.) whereas microcapillaries can be useful to isolate some specific sites and to investigate the behaviour of such sites at extremely high resolution (in the micrometer range).

The local measurements can also be used to monitor the modification of the passive film for example, during a forming process and the values obtained in the present study can be used as reference.

References

[1] H.S. Isaacs, M.W. Kendig, Corrosion 36 (1980) 269.
[2] R.S. Lillard, P.J. Moran, H.S. Isaacs, J. Electrochem. Soc. 139 (1992) 1007.
[3] F. Zou, D. Thierry, H.S. Isaacs, J. Electrochem. Soc. 144 (1997) 1957.
[4] E. Bayet, F. Huet, M. Keddam, K. Ogle, H. Takenouti, J. Electrochem. Soc. 144 (1997) L87.
[5] I. Annergren, D. Thierry, F. Zou, J. Electrochem. Soc. 144 (1997) 1208.
[6] L.V.S. Philippe, G.W. Walter, S.B. Lyons, J. Electrochem. Soc. 150 (2003) B111.
[7] G. Baril, C. Blanc, M. Keddam, N. Pébère, J. Electrochem. Soc. 150 (2003) B488.
[8] J.-B. Jorcin, E. Aragon, C. Merlatti, N. Pébère, Corros. Sci. 48 (2006) 1779.
[9] P. de Lima-Neto, J.P. Farias, L.F.G. Herculano, H.C. de Miranda, W.S. Araujo, J.-B. Jorcin, N. Pébère, Corros. Sci. 50 (2008) 1149.
[10] V.M.-W. Huang, V. Vivier, M.E. Orazem, N. Pébère, B. Tribollet, J. Electrochem. Soc. 154 (2007) C81.
[11] V.M.-W. Huang, V. Vivier, I. Frateur, M.E. Orazem, B. Tribollet, J. Electrochem. Soc. 154 (2007) C89.
[12] V.M.-W. Huang, V. Vivier, M.E. Orazem, N. Pébère, B. Tribollet, J. Electrochem. Soc. 154 (2007) C99.
[13] H. Bohni, T. Suter, F. Assi, Surf. Coat. Technol. 130 (2000) 80.
[14] R.A. Perren, T. Suter, P. Uggowitzer, L. Weber, R. Magdowski, H. Böhni, M. Speidel, Corros. Sci. 43 (2001) 707.
[15] R.A. Perren, T. Suter, P. Uggowitzer, L. Weber, R. Magdowski, H. Böhni, M. Speidel, Corros. Sci. 43 (2001) 727.
[16] T. Suter, R.C. Alkire, J. Electrochem. Soc. 148 (2001) B36.
[17] G. Castagnola, A. Squillace, M. Montuori, V. Marzocchi, V. Casanova, P. Mastronardi, G. Campanile, F. Bellucci, Adv. Mater. Res. 38 (2008) 320.
[18] T. Suter, T. Peter, H. Böhni, Mater. Sci. Forum 192 (1995) 25.
[19] T. Suter, H. Böhni, Electrochim. Acta 42 (1997) 3275.

[20] Y. Kobayashi, S. Virtanen, H. Böhni, J. Electrochem. Soc. 147 (2000) 155.
[21] H. Krawiec, V. Vignal, R. Oltra, Electrochem. Commun. 6 (2004) 655.
[22] H. Krawiec, V. Vignal, O. Heintz, R. Oltra, J.M. Olive, J. Electrochem. Soc. 152 (2005) B213.
[23] H. Krawiec, V. Vignal, O. Heintz, R. Oltra, Electrochim. Acta 51 (2006) 3235.
[24] H. Krawiec, V. Vignal, O. Heintz, R. Oltra, E. Chauveau, Metall. Mater. Trans. A 37 (2006) 1541.
[25] E. Angelini, B. De Benedetti, F. Rosalbino, Corros. Sci. 46 (2004) 1351.
[26] V. Vignal, N. Mary, R. Oltra, J. Peultier, J. Electrochem. Soc. 153 (2006) B352.
[27] H. Krawiec, V. Vignal, O. Heintz, P. Ponthiaux, F. Wenger, J. Electrochem. Soc. 155 (2008) C127.
[28] H. Krawiec, V. Vignal, R. Akid, Electrochim. Acta 53 (2008) 5252.
[29] N. Birbilis, B.N. Padgett, R.G. Buchheit, Electrochim. Acta 50 (2005) 3536.
[30] M. Pilaski, T. Hamelmann, A. Moehring, M.M. Lohrengel, Electrochim. Acta 47 (2002) 2127.
[31] M.M. Lohrengel, S. Heiroth, K. Kluger, M. Pilaski, B. Walther, Electrochim. Acta 51 (2006) 1431.
[32] I. Frateur, V.M.-W. Huang, M.E. Orazem, B. Tribollet, V. Vivier, J. Electrochem. Soc. 154 (2007) C719.
[33] M.E. Orazem, N. Pébère, B. Tribollet, J. Electrochem. Soc. 153 (2006) B129.
[34] J.-B. Jorcin, M.E. Orazem, N. Pébère, B. Tribollet, Electrochim. Acta 51 (2006) 1473.
[35] M.E. Orazem, B. Tribollet, Electrochemical Impedance Spectroscopy, The Electrochemical Society Series, John Wiley, 2008.